

Received April 5, 2017, accepted May 8, 2017, date of publication June 5, 2017, date of current version July 17, 2017.

Digital Object Identifier 10.1109/ACCESS.2017.2712131

# Neural-Network-Assisted UE Localization Using Radio-Channel Fingerprints in LTE Networks

XIAOKANG YE<sup>1</sup>, (Student Member, IEEE), XUEFENG YIN<sup>1</sup>, (Member, IEEE),  
XUESONG CAI<sup>1</sup>, (Student Member, IEEE),  
ANTONIO PÉREZ YUSTE<sup>2</sup>, (Senior Member, IEEE),  
AND HONGLIANG XU<sup>3</sup>

<sup>1</sup>College of Electronics and Information Engineering, Tongji University, Shanghai 201804, China

<sup>2</sup>School of Telecommunications Engineering, Technical University of Madrid, 28040 Madrid, Spain

<sup>3</sup>Shanghai Radio Monitoring Station, Shanghai 200031, China

Corresponding author: Xuefeng Yin (yinxuefeng@tongji.edu.cn)

This work was supported in part by the key project 5G Ka Frequency Bands and Higher and Lower Frequency Band Cooperative Trail System Research and Development of China Ministry of Industry and Information Technology under Grant 2016ZX03001015, in part by the Key Program of National Natural Science Foundation of China (NSFC) under Grant 61331009, in part by the general project of NSFC under Grant 61471268, in part by the HongKong, Macao, and Taiwan Science and Technology Cooperation Program of China under Grant 2014DFT10290, and in part by the project Development of a Performance Evaluation System for Localization Techniques/Equipments Utilizing Time-Difference-of-Arrival Information of Shanghai Radio Monitoring Station.

**ABSTRACT** In this paper, a novel fingerprint-based localization technique is proposed, which is applicable for positioning user equipments (UEs) in cellular communication networks such as the long-term-evolution (LTE) system. This technique utilizes a unique mapping between the characteristics of a radio channel formulated as a fingerprint vector and a geographical location. A feature-extraction algorithm is applied to selecting channel parameters with non-redundant information that are calculated from the LTE down-link signals. A feedforward neural network with the input of fingerprint vectors and the output of UEs' known locations is trained and used by UEs to estimate their positions. The results of experiments conducted in an in-service LTE system demonstrate that by using only one LTE eNodeB, the proposed technique yields a median error distance of 6 and 75 meters in indoor and outdoor environments, respectively. This localization technique is applicable in the cases where the Global Navigation Satellite System (GNSS) is unavailable, e.g., in indoor environments or in dense-urban scenarios with closely spaced skyscrapers heavily blocking the line-of-sight paths between a UE and GNSS satellites.

**INDEX TERMS** Long-term-evolution, fingerprint, radio propagation, channel impulse response, multipath component, feature extraction, neural networks, user equipment localization.

## I. INTRODUCTION

Recently, an increased demand for location-based services motivates the development of accurate, efficient, and real-time localization techniques in both indoor and outdoor environments [1]–[5]. Global Navigation Satellite Systems (GNSSs), such as the Global Positioning System (GPS), are widely used to localize a User Equipment (UE) in outdoor environments [6], [7]. However, in the cases where thick clouds block out the GNSS signals, or UEs are in a building [8], the localization performance is deteriorated severely. Another category of localization techniques makes use of Cellular Network (CN) and Wireless Local Area Network (WLAN) [9]. They are important supplements to the GNSS-based localization techniques, especially in indoor

environments and some outdoor environments where the navigation signals are heavily attenuated due to cloud absorption, building blockages, and foliage shadowing.

The CN- and WLAN-assisted localization techniques can be categorized into three groups based on the underlying positioning methodologies: lateration-, angulation-, and fingerprint-based algorithms [10]. For the lateration-based algorithms, the parameters such as received signal strength indicator [11], [12], reference signal received power [13], time of arrival and time difference of arrival of transmitted signals [14]–[16], are used to calculate the distances from multiple sites with known geographical locations to the UE in order to estimate the UE's location [17]. The angulation-based algorithms are used to localize the UE by estimating

the angles of arrival of the signals received from at least two known sites [18], [19]. These two kinds of algorithms rely on an assumption that a sufficient number of reference sites are available. The performance of localization technique based on the two algorithms deteriorates dramatically when the signals arrive at the UE from non-Line-of-Sight (NLoS) multipaths, or when the multipath fading in a cluttered environment results in erroneous estimates of the angle-of-arrival parameters.

The fingerprint-based algorithms [10], [20], [21] usually include two phases, i.e. a training phase in which a fingerprint database is constructed and a localization phase in which the constructed database is applied to estimating UEs' locations. The *fingerprint* is referred to as a specific set of parameters, which provides a unique combination of parameter values with respect to a geographical location. The fingerprint can be visual images, acoustic waves, radio signals and movement characteristics [21]. Data collected by sensors in a UE, e.g. ambient sound, light, and colors at a location, can be applied to constructing the audio-visual fingerprint [22], [23]. The signal fingerprint is referred to as the characteristics of radio frequency signals or radio channels, e.g. received signal strength [24]–[29], properties extracted based on Channel Impulse Responses (CIRs) [30]–[32], a sequence of cell-IDs [33], etc.. The motion fingerprint refers to velocities and orientations measured by a UE utilizing accelerometers and compasses [34]. After the fingerprint database is obtained, a UE location is estimated by comparing the currently achieved fingerprint with the database through matching algorithms, e.g. probabilistic methods, *k*-Nearest-Neighbor (*k*NN) based methods, neural networks, support vector machines, and decision tree approaches [35]–[39].

It is worth mentioning that for the rapid growth of the CN and WLAN, the signal fingerprint has attracted considerable attention [39]–[46]. In Section II, a collection of existing signal-fingerprint-based localization techniques is reported, and their performances as well as resource consumption are remarked. However, a common drawback of these localization techniques is that the information in the underlying fingerprints is restricted to few properties such as channel gains and propagation delays of LoS multipaths. In many cases, these properties exhibit a significant ambiguity with respect to multiple adjacent UE locations, and such an ambiguity deteriorates the localization performance consequently.

In this paper, we define a new structure of signal fingerprint based on multiple channel parameters selected from a broader scope than the existing techniques. All these channel parameters can be calculated by using the down-link signals of an LTE network. A neural network obtained in a training period is applied to localizing UEs based on a fingerprint database. The main novelties and contributions of our work lie in: *i*) Different from the parameters used in the existing localization techniques, totally eleven channel parameters calculated based on both narrowband and wideband characteristics of radio channel are taken into account to construct a fingerprint. Especially, channel parameters calculated based on

characteristics of multipath components in channel are considered; *ii*) A feature-extraction algorithm is utilized to determine the most suitable fingerprint for an area of interest; *iii*) The performance of the proposed localization technique is for the first time validated by channel measurements performed in both indoor and outdoor scenarios.

The rest of paper is structured as follows. In Section II, the state-of-art of signal-fingerprint-based localization techniques is reviewed. In Section III, the eleven channel parameters calculated from CIRs are elaborated, and procedures of forming a so-called fingerprint matrix are introduced. Then how to determine a channel parameter subset based on the fingerprint matrix and to train a neural network for localization are explained in Section IV. In Section V, two measurement campaigns for evaluating the performance of the proposed localization technique are presented. Finally, conclusive remarks are addressed in Section VI.

## II. SIGNAL-FINGERPRINT-BASED LOCALIZATION TECHNIQUES REVISITED

A variety of studies on signal-fingerprint-based localization techniques has been reported in literature. Some important pieces of work are summarized in Table 1. The key features of these techniques are tabulated which include the underlying wireless technologies, the adopted fingerprint matching algorithms, the positioning accuracy achieved, the technique complexity and resource consumption, as well as the typical application scenarios. Note that the positioning accuracy usually refers to the positioning error distance. Lower the positioning error distance resulted, higher the accuracy can be achieved for the underlying localization technique.

To illustrate the accuracy reported in these localization techniques more clearly, Figures 1(a) and 1(b) display positioning error distances in a bar plot for indoor and outdoor scenarios respectively. It can be observed from Figure 1 that the order of magnitude of the positioning error distance in indoor scenarios is less than 6 meters while the most of localization techniques in outdoor scenarios exhibit the order of magnitude of almost 50 meters.

It is clear from Table 1 that the WLAN is commonly used for the indoor, and the CN is applied for both indoor and outdoor localization. For most of techniques, characteristics extracted from CIRs are taken into account when constructing a fingerprint. Multipath information can also be integrated as a part of the fingerprint [47]. Then, the *k*NN and neural network algorithms are widely used for the fingerprint matching. In addition, the probabilistic methods are found to take more time than other matching algorithms to collect a sufficient number of samples in order to construct a statistical distribution of a parameter [49]. The positioning error distance is observed to be higher for the outdoor than the indoor scenarios. It is noted that a trade-off is a vital consideration among localization accuracy, technique complexity and resource consumption to fairly evaluate a localization technique.

**TABLE 1.** A summary of the literature studying signal-fingerprint-based localization techniques.

Literature	Wireless Technology	Matching Algorithm	Accuracy	Complexity or Resource Consumption	Scenario
[24] 2005	GSM (Signal strength)	<i>k</i> WNN	A median error distance of 2.48 to 5.44 meters	Use up to 29 channels and 6 strongest cells	In urban buildings
[40] 2007	Fixed WiMax (CIR)	4NN;4WNN;SVM	Mean error distance: 53.3 meters (4NN) 43.4 meters (4WNN) 49.6 meters (SVM)	Use only one site-known BS; 3 Rx are set for reference	Urban outdoor
[41] 2008	Self-built Network, 4.5 GHz CF, 3 GHz BW (Complex or power value of CIR)	Neural Network	An error distance of 1 meter at 93% CDF	Neural network size: 45 input neurons, 65 hidden neurons, 1 output neuron	In a room
[47] 2008	CDMA2000 (Multipath strength)	Neural Network	A mean error distance of 217.93 meters in 67% of test time	Neural network size depends on the number of pilots; 25 pilots are used to locate	Highway, urban streets
[43] 2010	Self-built Network, 2.4 GHz CF (CIR)	Neural Network	An error distance of less than 1 meter for 90% data	Neural network size: 7 input neurons, 10 hidden neurons, 1 output neuron; Only 1 Rx is set for reference	Gold mine tunnel
[42] 2010	Self-built Network, 5 GHz CF, 60 MHz BW (CIR)	Nonparametric Kernel Regression	An error distance of about 1.5 meters	$O(D^2)$ , $D$ is fingerprint vector dimension	Campus building
[48] 2011	ZigBee (TDoA CIR)	Self-organization Map Learning	An error distance of 1.47 meters at 90% CDF	Use 6 BSs; Less calibration measurements	Automation laboratory
[33] 2011	GSM (Cell-ID)	Cell-ID Sequence Matching	Mean error distance is less than 20% of the cell-tower-based triangulation	Low complexity when implemented on phones	Urban streets
[49] 2012	GSM (RSSI)	Bayesian Estimation and <i>k</i> NN	Mean error distance: 42.43 meters (rural) 27.86 meters (urban)	Faster than other RSSI-based GSM techniques; 20-minute order calibration; Up to 7 cells are used	Outdoor
[26] 2012	WLAN (RSS)	Compressive Sensing and K-means clustering	An error distance of 2.7 meters at 90% CDF	Need 3 more access points; Less calibration measurements	In a room
[44] 2012	WLAN, 20 BW (CIR)	1NN	A median error distance of nearly 1.5 meters	Use 22 access points; Use 596 training points	3rd floor of campus building
[31] 2013	WLAN, 2.4 GHz CF, 100 MHz BW (RSS,CIR,CTF,FCF)	<i>k</i> NN	Mean error distance: 1.5 to 2.5 meters (Fixed Rx) 2 to 3 meters (Moving Rx)	Use only one channel	Campus building
[45] 2014	WLAN (CIR)	Compressive Sensing	A maximum error distance of less than 4 meters	Use 25 reference points and 4 access points; Less calibration measurements	Indoor
[32] 2014	WLAN (Entropy of the magnitude and phase of CTF)	3NN	An error distance of 6 meters at 90% CDF	Use 202 training points; Use 3 fixed access points; Less complexity than CTF	Campus academic building
[46] 2015	Self-built Network (Cross-correlation of CIR)	Least Squares-based Algorithm	A median error distance of 50 meters	Need a training vehicle; 3 Rx are set for reference	Urban outdoor

a) GSM: Global System for Mobile Communication; WiMax: World Inter-operability for Microwave Access; CDMA: Code-Division Multiple Access; CF: Carrier Center Frequency; BW: Bandwidth; Self-built network: Ad hoc wireless system deployed specifically for localization.

b) TDoA: Time Difference of Arrival; RSSI: Received Signal Strength Indicator; RSS: Received Signal Strength; CIR: Channel Impulse Response; Cell-ID: Physical Cell Identity; CTF: Channel Transfer Function; FCF: Frequency Coherence Function.

c) *k*NN: *k*-Nearest-Neighbor; *k*WNN: *k*-Weighted-Nearest-Neighbor; SVM: Support Vector Machine.

d) CDF: Cumulative Distribution Function; Tx: Transmitter; Rx: Receiver; BS: Base Station.

In the work presented here, we focus on designing a new signal-fingerprint-based localization technique using radio channel characteristics extracted from the radio signals in the LTE network. Our intention is to explore more refined channel characteristics, especially those related to multipath

dispersion behaviors. We expect to find a combination of sensible channel parameters that allows to unambiguously identify a geographical location. The technique should be applicable provided that the signals from a fixed network node, say LTE's eNodeBs are available, regardless of the

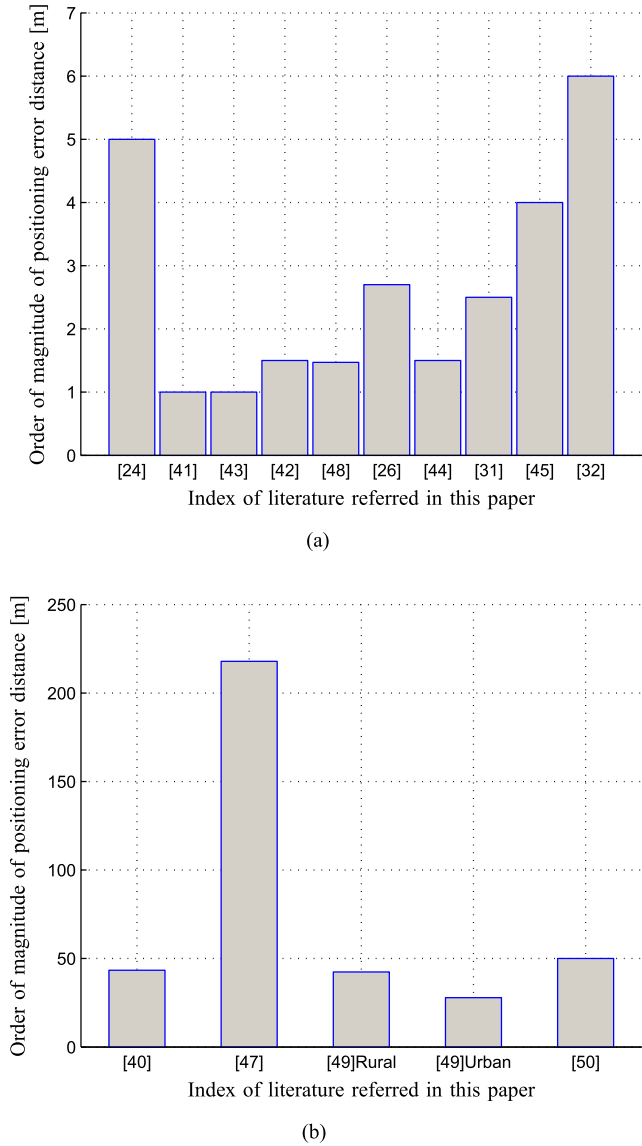


**Fig. 1.** The accuracy of localization techniques reported in the literature listed in Table 1. (a) Indoor scenarios. (b) Outdoor scenarios.

types of environments. The LTE network is particularly selected in the study here, as its down-link signals have a bandwidth of up to 20 MHz per carrier, which allows detecting multipath components (MPCs) in channel with an improved delay resolution [41]. To the authors' best knowledge, up to now, similar ideas of exploiting channel characteristics as the fingerprint for localization in LTE networks have been rarely studied [50], [51].

### III. CHANNEL-IMPULSE-RESPONSE-BASED FINGERPRINT

#### A. PROPOSED STRUCTURE OF A NOVEL SIGNAL FINGERPRINT

We assume that a UE utilizing the proposed signal-fingerprint-based localization technique can access a fingerprint database or a local storage from a physical cell of a base station (BS), e.g. an eNodeB of the LTE network.

The UE receives radio signals from the BS in service, and CIRs are extracted from common pilot signals, i.e. cell-specific reference signals of the LTE system by following the procedures proposed in [52]. A certain number of CIR-based channel parameters which are applicable for a specific environment are used as the fingerprint. The UE obtains its estimated location by comparing the current fingerprint with the existing fingerprint database. The database consists of the fingerprints obtained during the training period in the area that is covered by the radio signals transmitted from the cell. When accessing another cell, the UE chooses the fingerprint database of the new cell accordingly. To obtain the latest environmental changes, the fingerprint database is required to be updated in a regular manner by re-collecting the fingerprints for the area. The updating rate for the fingerprint database depends on the UE appearance frequency in the area, e.g. the database update is usually performed more frequently in urban than in mountainous, suburban or rural areas since the distribution or number of objects around the UE in the urban scenarios are more likely to change in a short period. In addition, both a commercial UE and a device dedicated for localization that own a high computational performance are recommended to update the fingerprint database under specifically designed protocols for necessary operations.

Besides the channel parameters calculated from CIR profiles, an algorithm called Space-Alternating Generalized Expectation-maximization (SAGE) is applied to extracting dominant MPCs in channel [53], [54]. Thanks to an availability of CIRs in various CNs and WLANs, the fingerprint can be composed of the channel parameters calculated from both CIR profiles and MPCs. Specifically, in our study, the proposed signal fingerprint is established based on eleven channel parameters that can provide a comprehensive understanding of the UE ambience. Table 2 lists these parameters which can be conveniently categorized into three groups describing respectively, channel fading behaviors, channel dispersive behaviors in delay domain observed based on CIRs, and more refined structures of CIRs represented by MPCs. Under the assumption that a UE is able to obtain these eleven channel parameters, it is possible to form a vector containing some of these parameters as an identity, i.e. a unique fingerprint vector for a location denoted with

$$\boldsymbol{\alpha}_z \triangleq [\hat{\theta}_{z1}, \hat{\theta}_{z2}, \dots, \hat{\theta}_{zs}, \dots, \hat{\theta}_{zJ}|(X_z, Y_z)], \quad (1)$$

where  $\hat{\theta}_{zs}$ ,  $s = 1, \dots, J$  represents the estimated value of the  $s$ th parameter at the  $z$ th sampling location whose  $x$ - and  $y$ -coordinates are  $X_z$  and  $Y_z$  respectively. Note that the UE localization is performed in a plain in this study, implying that a UE location is marked with two components as  $x$ - and  $y$ -coordinates. In the case of outdoor localization, the  $x$ - and  $y$ -coordinates of UE location are represented by the GPS latitude and longitude respectively. For the indoor localization, the coordinate of UE location is expressed in meter in a coordinate system specifically set in an area, e.g. a hall of a building. In such a case, the two components

**TABLE 2.** The eleven channel parameters for constructing the proposed signal fingerprint.

Category	Symbol (Index)	Note	Unit
Channel fading behaviors	$\bar{\sigma}_{\text{rsrp}}$ (1)	average reference signal received power	-
	$\xi_{\sigma_{\text{rsrp}}}$ (2)	standard deviation of reference signal received power	-
	$\sigma_F$ (3)	standard deviation of multipath fading	dB
	$\bar{K}$ (4)	average $K$ -factor	dB
Delay spreads calculated from CIR profiles	$\bar{\sigma}_\tau$ (5)	average root-mean-square delay spread	second
	$\xi_{\sigma_\tau}$ (6)	standard deviation of root-mean-square delay spread	second
	$\bar{\sigma}'_\tau$ (7)	average excess delay spread	second
	$\xi'_{\sigma_\tau}$ (8)	standard deviation of excess delay spread	second
MPC-based parameters	$\delta_{\text{sage}}$ (9)	average dynamic range of multipath power	dB
	$N_{\text{eff}}$ (10)	average number of effective multipaths	-
	$\sigma_{\tau, \text{sage}}$ (11)	standard deviation of multipath-based root-mean-square delay spread	second

represent the distances from the current location to the origin of the coordinate system in north-south and west-east directions respectively. The fingerprint database of the cell is composed of such fingerprint vectors. Note that the proposed localization technique is scalable to include multiple nodes, and the single-node fingerprint can be extended into a multiple-node one. To this end, the channel parameters calculated based on down-link signals from multiple cells can be arranged in a vector for each location.

### B. CHARACTERISTICS EXTRACTED FROM CIRs

The time-division-duplexing frame of the LTE system is composed of twenty time-slots and lasts for totally ten milliseconds [55]. In our case, CIRs extracted from half-frame signals are regarded as one snapshot. Totally 200 snapshots of CIRs collected during one second are considered as an “observation segment”, and one fingerprint vector  $\alpha_z$  is then generated in which the eleven channel parameters are calculated. Notice that the location coordinates are recorded at the starts of individual one-second segments.

#### 1) AVERAGE AND STANDARD DEVIATION OF REFERENCE SIGNAL RECEIVED POWER

The so-called Reference Signal Received Power (RSRP) is a parameter for the LTE system which is defined as the

arithmetic mean over the power contribution of the cell-specific reference signals [55]. As an extension of this definition, in our case, the RSRP in the  $m$ th snapshot denoted by  $\gamma_m$  which is obtained from the effective normalized Power Delay Profile (PDP) in the  $m$ th snapshot  $P'_m(\tau)$  can be calculated as

$$\gamma_m = \int P'_m(\tau) d\tau. \quad (2)$$

The normalized PDP  $P_m(\tau)$  is calculated as

$$P_m(\tau) = \frac{|y_m(\tau)|^2}{\int |y_m(\tau')|^2 d\tau'}, \quad (3)$$

where  $y_m(\tau)$  is a complex-valued CIR in delay in the  $m$ th snapshot. The effective normalized PDP  $P'_m(\tau)$  can be obtained from the normalized PDP  $P_m(\tau)$  by preserving its spectral components that exceed a power threshold set for eliminating the influence of noises. Then the average and standard deviation of RSRP denoted by  $\bar{\sigma}_{\text{rsrp}}$  and  $\xi_{\sigma_{\text{rsrp}}}$  respectively are calculated based on all snapshots of RSRPs in one observation segment as

$$\begin{aligned} \bar{\sigma}_{\text{rsrp}} &= \frac{1}{M} \sum_{m=1}^M \gamma_m \\ \xi_{\sigma_{\text{rsrp}}} &= \text{std}(\gamma_m; m = 1, \dots, M) \\ &= \left( \frac{1}{M-1} \sum_{m=1}^M (\gamma_m - \bar{\sigma}_{\text{rsrp}})^2 \right)^{1/2}, \end{aligned} \quad (4)$$

where  $\text{std}(\cdot)$  is an operator for calculating the standard deviation of the given arguments, and  $M$  represents a total number of snapshots during one second, i.e. 200 snapshots in our case.

#### 2) STANDARD DEVIATION OF MULTIPATH FADING

We assume that a UE experiences constant path loss and shadow fading during one snapshot that lasts 5 milliseconds. Channel narrowband coefficient can be simply viewed as an indicator of multipath fading severity. According to [56], the channel narrowband coefficient in the  $m$ th snapshot denoted by  $h_m$  is calculated as

$$h_m = \int y_m(\tau) d\tau, \quad m = 1, \dots, M. \quad (5)$$

Then, the standard deviation of multipath fading denoted by  $\sigma_F$  is calculated as the standard deviation of  $|h_m|^2$  in a logarithmic form in one observation segment, i.e.

$$\sigma_F = \text{std}\left(10 \cdot \log_{10}(|h_m|^2); m = 1, \dots, M\right). \quad (6)$$

#### 3) AVERAGE $K$ -FACTOR

The so-called  $K$ -factor is defined as a ratio between the power of deterministic and of scattering components [57]. For the CIRs obtained in  $M_k$  snapshots in each of  $N$  segments,  $K$ -factor can be calculated based on the observations obtained from these  $M_k$  snapshots. In the  $n$ th segment, the response of the deterministic component can be obtained by averaging the complex-valued CIRs while the response of the scattering

component by subtracting the average CIRs from the individual CIRs. Then the narrowband representations of two components denoted by  $h_{\text{det},n}$  and  $h_{\text{sca},m,n}$ ,  $m = 1, \dots, M$  respectively are calculated by the same way of (5). Then the  $K$ -factor in the  $n$ th segment denoted by  $K_n$  is calculated as

$$K_n = 10 \cdot \log_{10} \left\{ |h_{\text{det},n}|^2 \left( \frac{1}{M_k} \sum_{m=1}^{M_k} |h_{\text{sca},m,n}|^2 \right)^{-1} \right\}, \quad (7)$$

where  $M_k$  is associated with the coherence time during which the radio channel is considered time-invariant, and moreover,  $M_k \cdot N = 200$  in our case. Here,  $M_k$  is set 10, i.e. the channel is regarded time-invariant in 50 milliseconds. The average  $K$ -factor denoted by  $\bar{K}$  is calculated as  $\bar{K} = \frac{1}{N} \sum_{n=1}^N K_n$ .

#### 4) AVERAGE AND STANDARD DEVIATION OF ROOT-MEAN-SQUARE DELAY SPREAD

The so-called root-mean-square (rms) delay spread describes the dispersive behaviors of MPCs in the delay domain attributed to the UE's surroundings. Note that the received signals are the convolution among the responses of transmitter and receiver as well as the radio channel. As a consequence, an MPC's delay may be different from the delay caused by the radio propagation. For this reason, we choose the delay spread to characterize channel dispersion in the delay domain rather than the MPC delay in the case where the time instant for transmitting signals is unknown to the receiver, i.e. the UE in our case. According to [58], the rms delay spread in the  $m$ th snapshot denoted by  $\sigma_{\tau,m}$  is calculated based on the second central moment of the effective normalized PDP  $P'_m(\tau)$  in the  $m$ th snapshot as

$$\sigma_{\tau,m} = \sqrt{\int (\tau - \bar{\tau}_m)^2 P'_m(\tau) d\tau}, \quad m = 1, \dots, M, \quad (8)$$

with

$$\bar{\tau}_m = \int \tau P'_m(\tau) d\tau. \quad (9)$$

Then the average and standard deviation of rms delay spread denoted by  $\bar{\sigma}_{\tau}$  and  $\xi_{\sigma_{\tau}}$  respectively are calculated based on the  $M$  snapshots of CIRs during one observation segment.

#### 5) AVERAGE AND STANDARD DEVIATION OF EXCESS DELAY SPREAD

Another way to describe the channel dispersive behaviors in the delay domain is presented as delay scope within which the MPCs are considered dominant [59]. We need to specify a power threshold, e.g. 10 dB above the spectral height of the noise components, or 10 dB below the highest power in delay. The normalized PDP whose spectral heights within a certain delay range are above this threshold will be considered as signal components. The part of PDP below this threshold is considered to be insignificant. The so-called excess delay spread is then defined to be the range of the signal components in the delay domain. Then the average and standard deviation of excess delay spread denoted by  $\bar{\sigma}'_{\tau}$  and  $\xi'_{\sigma_{\tau}}$  respectively

are calculated based on the  $M$  snapshots of CIRs during one observation segment.

#### C. MULTIPATH-COMPONENTS-BASED CHARACTERISTICS EXTRACTED BY USING THE SAGE ALGORITHM

The SAGE algorithm, an approximation of the maximum likelihood estimation algorithm, has been applied to estimating the MPCs' parameters by using an iterative approach. In our case, each MPC is characterized by the parameters of the complex-valued amplitude and delay. The CIR  $y(t)$  can be written in the form of the superposition of the MPCs in channel as

$$y(t) = \sum_{\ell=1}^L a_{\ell} \delta(t - \tau_{\ell}) + n(t), \quad (10)$$

where  $L$ ,  $a_{\ell}$  and  $\tau_{\ell}$  denote respectively the total number of MPCs, the amplitude and the delay of the  $\ell$ th MPC in channel, and  $n(t)$  represents the complex white Gaussian noise components.

Based on the estimated parameters of MPCs from multiple snapshots in one observation segment, three channel parameters are calculated and considered to be useful for constructing a fingerprint, which are:

- Average dynamic range of multipath power over one observation segment denoted by  $\delta_{\text{sage}}$ . The difference between the strongest power and the weakest power of MPCs for the  $m$ th snapshot is denoted by  $\Delta P_m$ , and then, the parameter  $\delta_{\text{sage}}$  is calculated as the arithmetic mean over all the  $M$  snapshots as  $\delta_{\text{sage}} = \frac{1}{M} \sum_{m=1}^M \Delta P_m$ ;
- Average number of effective multipaths over one observation segment denoted by  $N_{\text{eff}}$ . Here, the effective multipaths refer to the MPCs with power larger than two times of the noise spectral height. When denoting the number of effective multipaths in the  $m$ th snapshot by  $N_{\text{eff},m}$ , the parameter  $N_{\text{eff}}$  is calculated as  $N_{\text{eff}} = \frac{1}{M} \sum_{m=1}^M N_{\text{eff},m}$ ;
- Standard deviation of multipath-based rms delay spread denoted by  $\sigma_{\tau,\text{sage}}$ . This parameter is obtained by calculating the standard deviation of the delay spreads for all the snapshots during one observation segment.

It is worth mentioning that the standard deviation of rms delay spread extracted from both CIR profiles and MPCs, i.e.  $\xi_{\sigma_{\tau}}$  and  $\sigma_{\tau,\text{sage}}$  are defined in a similar way. The CIR profiles provide an overall information of the radio channel while the MPCs represent dominant components in the channel. Preserving these two parameters at the same time is necessary for constructing an accurate and informative fingerprint.

#### D. FINGERPRINT MATRIX FORMED BY CHANNEL PARAMETERS

In our localization technique, a fingerprint matrix denoted by  $\mathbf{F}$  is introduced which is used in both the training and localization phases. This 2-dimension matrix is with rows and columns being the sampling locations and the channel parameters respectively. We denote the fingerprint matrices for the

training and localization phases by  $\mathbf{F}_{\text{tp}}$  and  $\mathbf{F}_{\text{lp}}$  respectively. In this subsection, the procedure of generating a fingerprint matrix is elaborated.

Note that the channel parameters which are calculated as in subsections III-B and III-C do not have the same unit, e.g. the multipath fading in a logarithmal form and the delay spread in seconds. Moreover, the orders of magnitude of two channel parameters are likely to be dramatically different, e.g. the delay spread of  $10^{-7}$  seconds and the average number of effective multipaths of 10. As a result, the influence of channel parameter with less order of magnitude may be easily neglected in the further step of feature extraction. Therefore, to construct a fingerprint vector with multiple elements, it is important to harmonize the unit and order of magnitude of each channel parameter through certain transformation operations.

Firstly, in the form of the fingerprint vector  $\boldsymbol{\alpha}$  in (1), we introduce a matrix  $\mathbf{X}$  which is obtained by concatenating the channel parameters as well as the coordinates of  $C$  sampling locations for an area in columns. The matrix  $\mathbf{X}$  which can be split into two matrices  $\mathbf{V}$  and  $\mathbf{G}$  is written as

$$\begin{aligned} \mathbf{X} &= [\boldsymbol{\alpha}_1 \quad \boldsymbol{\alpha}_2 \quad \cdots \quad \boldsymbol{\alpha}_C]^T \\ &\triangleq [\mathbf{V} \mid \mathbf{G}], \end{aligned} \quad (11)$$

with

$$\mathbf{V} = \begin{bmatrix} \hat{\theta}_{11} & \hat{\theta}_{12} & \cdots & \hat{\theta}_{1J} \\ \hat{\theta}_{21} & \hat{\theta}_{22} & \cdots & \hat{\theta}_{2J} \\ \vdots & \vdots & \ddots & \vdots \\ \hat{\theta}_{C1} & \hat{\theta}_{C2} & \cdots & \hat{\theta}_{CJ} \end{bmatrix} \quad (12)$$

and

$$\mathbf{G} = \begin{bmatrix} X_1 & Y_1 \\ X_2 & Y_2 \\ \vdots & \vdots \\ X_C & Y_C \end{bmatrix}, \quad (13)$$

where  $(\cdot)^T$  is an operator for obtaining the transpose of the given matrix. The matrix  $\mathbf{G}$  is a so-called location matrix in which each row represents the coordinate of a sampling location. A location matrix denoted by  $\mathbf{G}_{\text{tp}}$  is composed of the coordinates of sampling locations in the training phase, while another location matrix denoted by  $\mathbf{G}_{\text{lp}}$  contains the coordinates of the locations to be estimated in the localization phase.

Two steps are performed to transform the matrix  $\mathbf{V}$  into the fingerprint matrix  $\mathbf{F}$ . Removing average and scaling standard deviation to unit are used in order to transform the elements of each column in the matrix  $\mathbf{V}$  into random variables with zero mean and unit standard deviation. It is noted that the elements in the matrix  $\mathbf{F}$  unnecessarily vary within the scope of  $-1$  to  $1$  after these transformations.

*Step 1 (Removing Average):* The arithmetic average over elements in each column of the matrix  $\mathbf{V}$  is removed. An auxiliary matrix  $\mathbf{Q}$  with  $C$  rows and  $J$  columns is calculated as

$$\mathbf{Q} = \mathbf{V} - \mathbf{1}\boldsymbol{\beta}, \quad (14)$$

where  $\mathbf{1}$  denotes a column vector containing  $C$  elements of 1's, and  $\boldsymbol{\beta}$  denotes a row vector containing the averages in each row of  $\mathbf{V}$ , i.e.  $\boldsymbol{\beta} = [\frac{1}{C} \sum_{i=1}^C v_{i1}, \dots, \frac{1}{C} \sum_{i=1}^C v_{ij}, \dots, \frac{1}{C} \sum_{i=1}^C v_{iJ}]$ , where  $v_{ij}$  denotes the  $(i, j)$ th element of the matrix  $\mathbf{V}$ .

*Step 2 (Scaling Standard Deviation to Unit):* The standard deviation of elements in each column of the matrix  $\mathbf{Q}$  is scaled to one. The matrix  $\mathbf{F}$  with  $C$  rows and  $J$  columns is calculated as

$$\mathbf{F} = \mathbf{Q}\mathbf{D}^{-1}, \quad (15)$$

where  $(\cdot)^{-1}$  denotes an inverse of the given matrix, and  $\mathbf{D}$  is an auxiliary diagonal matrix defined as

$$\mathbf{D} \triangleq \text{diag}(\text{std}(q_{ij}; i = 1, \dots, C; j = 1, \dots, J)) \quad (16)$$

with  $q_{ij}$  being the  $(i, j)$ th element of the matrix  $\mathbf{Q}$ , where  $\text{diag}(\cdot)$  denotes an operator for constructing a diagonal matrix with diagonal elements being the given arguments.

#### IV. FINGERPRINT-BASED LOCALIZATION TECHNIQUE

In this section, a feature-extraction algorithm and a neural network algorithm used in the proposed localization technique are introduced. For the training phase, a feature-extraction algorithm is implemented which selects  $J_0$  columns from the fingerprint matrix  $\mathbf{F}_{\text{tp}}$ , e.g. the first and the fifth columns. Then a new matrix  $\mathbf{F}'_{\text{tp}}$  with two columns is constructed. In such a case, a subset with the first and the fifth channel parameters is determined from the original parameter set. Then a feed-forward neural network is trained with the input of the matrix  $\mathbf{F}'_{\text{tp}}$  and the output of the location matrix  $\mathbf{G}_{\text{tp}}$ . For the localization phase, a matrix  $\mathbf{F}'_{\text{lp}}$  is obtained by selecting the first and the fifth columns from the matrix  $\mathbf{F}_{\text{lp}}$ . The location estimation is performed by using the trained neural network. Finally, a matrix  $\hat{\mathbf{G}}_{\text{lp}}$  generated using the neural network whose elements are estimated coordinates of the locations is compared with the location matrix  $\mathbf{G}_{\text{lp}}$  for calculating the positioning error distances.

##### A. FEATURE EXTRACTION FOR THE FINGERPRINT MATRIX

The feature-extraction algorithm is used to select a feature subset from a set of features, considering their relevance and redundancy [60]. A good feature subset is defined in which the features are weakly relevant from each other and remain non-redundant [61]. This principle is applied in our case to selecting a channel parameter subset based on the matrix  $\mathbf{F}_{\text{tp}}$ .

The relevance among channel parameters is closely related to the types of environments [62]. Some parameters are significantly relevant in a certain environment, and become less relevant in another case. Thus, for each specific area, it is necessary to select a subset of the eleven channel parameters for establishing fingerprint vectors. Moreover, the computational complexity required for matrix operation is reduced by using a subset of parameters in both training and localization phases.

Here, we briefly introduce the proposed feature-extraction algorithm based on the entropy and information gain [63].

This algorithm is theoretically convinced and practically simple [60].

Firstly, a Singular Value Decomposition-based (SVD-) entropy of a matrix  $\mathbf{Z}$  is defined as an entropy of normalized eigenvalues of the matrix  $\mathbf{Z}\mathbf{Z}^T$  [63]. The normalized eigenvalue of the  $j$ th column denoted by  $\omega_j$  is calculated as

$$\omega_j = \frac{s_j^2}{\sum_k s_k^2}, \quad (17)$$

where  $s_j$  represents the  $j$ th singular value of the matrix  $\mathbf{Z}$ . According to [63], the SVD-entropy of the matrix  $\mathbf{Z}$  denoted by  $E(\mathbf{Z})$  is calculated as

$$E(\mathbf{Z}) = -\frac{1}{\log(R)} \sum_{j=1}^R \omega_j \log(\omega_j), \quad (18)$$

where  $R$  is the rank of the matrix  $\mathbf{Z}$ . The SVD-entropy varies between 0 and 1. If the SVD-entropy equals zero, the matrix  $\mathbf{Z}$  can be expressed by a single eigenvector of the matrix  $\mathbf{Z}\mathbf{Z}^T$ , i.e. one normalized eigenvalue in the matrix  $\mathbf{Z}$  is 1 and the others are zeros. If the SVD-entropy equals one, the matrix can be expressed by all the eigenvectors of the matrix  $\mathbf{Z}\mathbf{Z}^T$ , i.e.  $\omega_j = \frac{1}{R}$  for all  $j$  in the matrix  $\mathbf{Z}$ . In our case, the SVD-entropy of 0 implies that only a single channel parameter in a certain set is significant, while the SVD-entropy of 1 means that all the channel parameters in a certain set are equally important.

Secondly, we introduce a new matrix  $\mathbf{W}$  to distinguish from the previous matrix  $\mathbf{Z}$ . Note that  $\mathbf{W}[-i]$  represents the matrix obtained by removing the  $i$ th column from the matrix  $\mathbf{W}$ . A contribution of the  $i$ th feature to the SVD-entropy of the matrix  $\mathbf{W}$  defined in [64] is written as

$$\lambda_i = E(\mathbf{W}) - E(\mathbf{W}[-i]), \quad i = 1, \dots, J. \quad (19)$$

Hereby, we call  $\lambda_i$  the contribution of the feature to the entropy which is termed as *CE-Value*. In some literature, the CE-Value is also called information gain, which indicates the importance of one feature to the original feature set. If the SVD-entropy of the matrix  $\mathbf{W}[-i]$  is less than that of the matrix  $\mathbf{W}$ , the  $i$ th feature is vital and considered to be reserved in the feature subset, otherwise, the  $i$ th feature can be removed from the feature subset. One can select a feature whose CE-Value is positive. However, the situation that all the feature CE-Values in the original feature set are positive may occur. As an alternative, to extract the dominant features we recommend to consider the average and standard deviation of the feature CE-Values in the original set. We denote the average and standard deviation of all the feature CE-Values by  $\lambda_{avg}$  and  $\lambda_{std}$  respectively. The feature whose CE-Value is higher than  $\lambda_{avg} + \lambda_{std}$  is called an entropy-contributing feature. The total number of entropy-contributing features is regarded as the size of the feature subset, i.e. a combination of channel parameters. Here, four approaches of the algorithm proposed in [65] are utilized to determine a final feature subset, i.e. Simple Ranking (SR), the first Forward

Selection (FS1), the second Forward Selection (FS2) and Backward Elimination (BE).

We evaluate the performance of the underlying feature-extraction approaches by using two metrics. One is the Sammon's error applied to showing the preservation extent of the structure in the dimension-reduced matrix by using the Euclidean distance between two samples of the matrix [65], i.e. two rows in the matrix  $\mathbf{F}'_{tp}$  in our case. Lower the Sammon's error value, a better preservation is achieved. The Sammon's error denoted by  $\mu$  is defined as

$$\mu = \frac{1}{\sum_{i < j} \tilde{d}_{ij}} \sum_{i < j} \frac{(\tilde{d}_{ij} - d_{ij})^2}{\tilde{d}_{ij}}, \quad (20)$$

where  $\tilde{d}_{ij}$  denotes the Euclidean distance between two samples  $\tilde{\mathbf{w}}_i$  and  $\tilde{\mathbf{w}}_j$  in the dimension-reduced matrix  $\tilde{\mathbf{W}}$  while  $d_{ij}$  represents the Euclidean distance between two samples  $\mathbf{w}_i$  and  $\mathbf{w}_j$  in the matrix  $\mathbf{W}$ . Another metric is the correlation coefficient which is introduced to address a linear dependency of two features, i.e. two channel parameters in our case [66]. The correlation coefficient  $\rho(\beta_i, \beta_j)$  between two channel parameters, say  $\beta_i$  and  $\beta_j$ , is calculated as

$$\rho(\beta_i, \beta_j) = \frac{\text{Cov}(\beta_i, \beta_j)}{(\text{D}(\beta_i) \cdot \text{D}(\beta_j))^{1/2}} \quad (21)$$

with

$$\text{Cov}(\beta_i, \beta_j) = \bar{E}([\beta_i - \bar{E}(\beta_i)][\beta_j - \bar{E}(\beta_j)]), \quad (22)$$

where  $\bar{E}(\cdot)$  and  $D(\cdot)$  denote respectively two operators for calculating the expectation and variance of the given argument. To determine which feature-extraction approach is used, both two metrics should be considered, and a composite metric denoted by  $\Lambda$  is introduced to combine the Sammon's error and the absolute value of correlation coefficient. The metric  $\Lambda$  is defined for each feature-extraction approach as

$$\Lambda = \mu + \sum_{i < j} |\rho(\beta_i, \beta_j)|, \quad 1 \leq i, j \leq J, \quad (23)$$

where  $|\cdot|$  denotes the absolute value of the given argument. In our case, the channel parameter subset is chosen by using the feature-extraction approach with the lowest value of  $\Lambda$ .

## B. LOCALIZATION USING A NEURAL-NETWORK-BASED APPROACH

The neural network is a software technique analogous to a brain in the biology. The neural network is usually trained to perform a matching between a specific input and a target output in many applications, e.g. classification, pattern recognition, dynamic control [67]. A neural network is comprised of a number of basic elements called *neuron*. In order to train the network, a learning algorithm is applied to updating both connections between the neurons and neuron thresholds until the output of the network is as consistent as possible with the target output. Specifically, a neural network for a particular learning task is trained based on a group of known samples

with label, and predicts the output of the network with the test samples. It is a widely investigated approach to learning a pattern that reveals a non-linear relationship between the known input and target output, which makes the fingerprint-based localization feasible using a neural network [68].

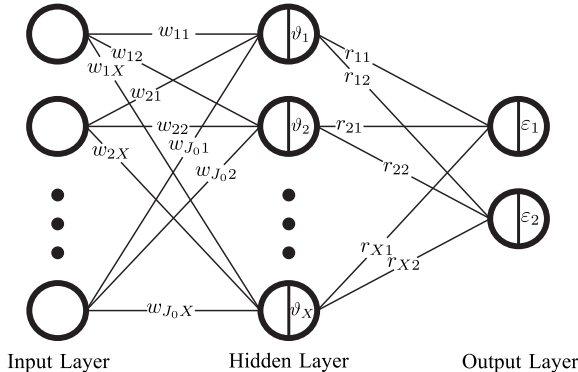


**Fig. 2.** The structure of the feed-forward neural network with the input, hidden and output layers for each sampling location.

In this paper, a neural network with feed-forward architecture and an error-back-propagation-based learning algorithm is adopted. This kind of neural network usually contains three layers each with a number of neurons, i.e. an input layer, a hidden layer, and an output layer. The term “feed-forward” implies that the neural network has a topological structure in which only links between two neighboring layers exist, i.e. the input layer can only be connected to the hidden layer while the hidden layer only to the output layer. In our case, the neural network to be trained has a pair of input and output, i.e. the fingerprint matrix  $\mathbf{F}'_{\text{tp}}$  and the location matrix  $\mathbf{G}_{\text{tp}}$  respectively. Specifically, the input matrix  $\mathbf{F}'_{\text{tp}}$  is composed of  $C$  sampling locations organized as rows each consisting of  $J_0$  elements representing channel parameters, and the output matrix  $\mathbf{G}_{\text{tp}}$  contains correspondingly  $C$  sampling locations with their two coordinate components. The number of neurons in the input layer denoted by  $N_{\text{input}}$  is equal to the number of columns in  $\mathbf{F}'_{\text{tp}}$ . Similarly, the number of neurons in the output layer denoted by  $N_{\text{output}}$  is set identical with the number of columns in  $\mathbf{G}_{\text{tp}}$ . Nevertheless, the number of neurons in the hidden layer denoted by  $N_{\text{hidden}}$  is adaptive [69]. To determine  $N_{\text{hidden}}$ , we attempt to run the neural network with  $N_{\text{hidden}}$  ranging from 2 to 10, and the trained neural network is chosen which yields the minimal positioning error distance.<sup>1</sup> Figure 2 illustrates the structure of the feed-forward three-layer neural network implemented in our case. The circles in this figure represent neurons in different layers. For convenience of description, those neurons are called “input-layer-neurons”, “hidden-layer-neurons” and “output-layer-neurons” respectively. In our case, each input-layer-neuron represents a selected channel parameter after feature-extraction while two

<sup>1</sup>A comprehensive guidance of determining the neuron quantity can be referred to [70].

output-layer-neurons denote the two components of the location coordinate respectively. An activation function  $y_0 = f(x_0)$  is used to calculate the output of the hidden-layer-neuron or the output-layer-neuron  $y_0$ . The input  $x_0$  of the activation function is the difference between a neuron’s input and its own threshold. The choice of our activation functions used in the hidden layer and output layer will be discussed later.

An error-back-propagation algorithm defined based on a first-order method proposed in [71] has been widely studied. This algorithm requires a large number of iterations to obtain the neural network convergence [72]. Some improved error-back-propagation algorithms, e.g. two second-order methods of neuron by neuron [73] and of Levenberg-Marquardt (LM) [74] as well as regular Bayesian method, provide a better prediction accuracy with a low complexity. Among them, despite of a computational complexity in processing a large-size network that usually contains thousands of neurons, the second-order LM algorithm for a medium-size network needs much less iterations with lower Mean Squared Error (MSE) compared with the first-order error-back-propagation algorithm. We apply the LM algorithm to train the proposed feed-forward neural network. The MSE calculated based on an objective function in this algorithm is considered as a metric to assess an error between the output of the neural network and the exact counterpart known in advance. The connection weight between the two neurons and the threshold of a neuron are adjusted iteratively by minimizing the MSE. We use  $\mathbf{a}_i$  and  $\mathbf{b}_i$  to denote the attribute vector and the label vector respectively in the  $i$ th training instance, i.e. a  $J_0$ -dimension fingerprint vector and a 2-dimension vector for a sampling location in our case. A training set for the neural network denoted by  $\mathbb{T}$  that contains multiple training instances is written as

$$\mathbb{T} = \{(\mathbf{a}_i, \mathbf{b}_i) | i = 1, \dots, C\}, \quad (24)$$

where  $\mathbf{b}_i = (b_{i,1}, b_{i,2})$  is the exact output in the  $i$ th training instance. Supposing that the final output of the neural network in the  $i$ th training instance is  $\hat{\mathbf{b}}_i = (\hat{b}_{i,1}, \hat{b}_{i,2})$ . The error of the  $i$ th training instance denoted by  $\delta_{\text{err}}^i$  is calculated as

$$\delta_{\text{err}}^i = (\hat{b}_{i,1} - b_{i,1})^2 + (\hat{b}_{i,2} - b_{i,2})^2. \quad (25)$$

The MSE of the whole training set to be minimized, say  $\delta_{\text{err}}$ , is calculated as

$$\delta_{\text{err}} = \frac{1}{C} \sum_{i=1}^C \delta_{\text{err}}^i. \quad (26)$$

A neuron-parameter vector  $\kappa$  in our case is defined as  $\kappa = (w_{11}, \dots, w_{J_0X}, r_{11}, \dots, r_{X2}, \vartheta_1, \dots, \vartheta_X, \varepsilon_1, \varepsilon_2)$ . The updated  $\kappa$  value denoted by  $\kappa'$  can be written as

$$\kappa' = \kappa + \Delta\kappa, \quad (27)$$

with the adjustment  $\Delta\kappa$  calculated as

$$\Delta\kappa = -(\mathbf{J}^T \mathbf{J} + \epsilon \mathbf{U})^{-1} \mathbf{J}^T \mathbf{e}, \quad (28)$$

**TABLE 3.** Settings of learning parameters of the neural network based on the Levenberg-Marquardt algorithm in the cases considered here.

Setting	Value
Number of Neurons in Input Layer	$J_0$
Number of Neurons in Output Layer	2
Activation Function of Hidden Layer	Tangent-Sigmoid
Activation Function of Output Layer	Linear
Training Algorithm	Levenberg-Marquardt
Learning Rate	0.03
Performance Function	Mean Squared Error
Goal Performance	$1 \times 10^{-2}$ (indoor) $1 \times 10^{-8}$ (outdoor)
Performance Function Minimum Gradient	$1 \times 10^{-2}$ (indoor) $1 \times 10^{-8}$ (outdoor)
Iteration	300
Maximum Validation Check	10

where  $\mathbf{U} \in \mathbb{R}^{D \times D}$ ,  $D = J_0 \times X + 2 \times X + X + 2$  is an identity matrix,  $\mathbf{J}$  is a Jacobian matrix with  $C \times 2$  rows and  $D$  columns whose elements are derived from the gradient of the MSE,  $\epsilon$  is a learning rate, and  $e = (\hat{\mathbf{b}}_1 - \mathbf{b}_1, \dots, \hat{\mathbf{b}}_i - \mathbf{b}_i, \dots, \hat{\mathbf{b}}_C - \mathbf{b}_C)$  is a row vector with regard to all the training instances [75].

In practice, we use MATLAB Neural Network Toolbox<sup>2</sup> to construct a feed-forward three-layer neural network using the LM algorithm. Table 3 displays the parameters for establishing the proposed neural network. The tangent-sigmoid function and linear function are selected as activation functions of the hidden layer and the output layer respectively, which are defined as

$$f_h(x) = \frac{2}{1 + e^{-2x}} - 1, \quad (29)$$

$$f_o(x) = x. \quad (30)$$

Note that a linear function is chosen as the activation function of the output layer since it can retain the input undistorted regardless of location coordinates. The training for the neural network is ceased if any of the following conditions is satisfied:

- For outdoor localization, the MSE performance is set less than  $1 \times 10^{-8}$ . For examples, if the error in the longitude estimate is  $10^{-4}$  degrees, the error of straight-line distance grows from 4.166 meters to 11.077 meters in the cases of the latitude decreasing from 68 degrees to 5 degrees. For indoor localization, the MSE of less than  $1 \times 10^{-2}$  meters implies a straight-line distance of 0.14 meters between two locations.
- The gradient of the MSE is less than  $1 \times 10^{-2}$  or  $1 \times 10^{-8}$  for indoor and outdoor localization respectively.
- The MSE keeps increasing in more than 10 iterations.
- The maximum iteration number reaches 300.

<sup>2</sup>The details of the Neural Network Toolbox in MATLAB software can be referred to <https://cn.mathworks.com/products/neural-network/index.html>

Changing the above settings can influence the accuracy of the neural network algorithm. It is necessary to seek a balance between a computational complexity and a tolerable positioning error level. Our experimental results shown later in Section V illustrate that the current settings are appropriate to maintain reasonable accuracy with a tractable complexity.

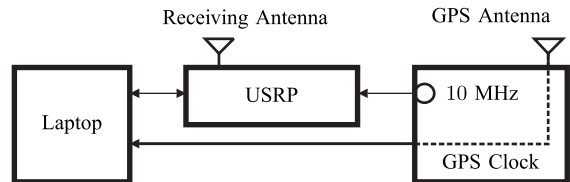


**Fig. 3.** The architecture of the three-part channel measurement system.

## V. MEASUREMENT CAMPAIGNS AND LOCALIZATION PERFORMANCE

We performed two channel measurement campaigns in an indoor and an outdoor environments respectively, using a suit of Universal Software-defined Radio Peripheral (USRP) device controlled by a software. Figure 3 illustrates the diagram of the measurement system which consists of, besides the USRP, a laptop computer carrying a storage disk, an omnidirectional antenna working in 1-3 GHz LTE operating frequency band, and a GPS-disciplined clock generating a sinusoidal signal with the frequency of 10 MHz. The USRP connected with the antenna is controlled by the laptop and used to output the baseband data. The GPS-disciplined clock provides reference timing signals to avoid the oscillator drifts in the USRP. Furthermore, it also provides the latitude and longitude information for the outdoor measurements. The geographical information is used as the target output of the neural network in the training phase, and is also regarded as the true values in the localization phase for assessing the accuracy of the localization technique. The down-link LTE signals with a bandwidth of 20 MHz are acquired with a sampling rate of 50 Msample/s in all the measurements.

It is worth mentioning that in the outdoor environments, the LoS propagation scenario is usually obtained. In such a case, the channels observed at different UE locations exhibit similar CIRs which are hard to distinguish. Such an ambiguity results in the low accuracy of the proposed localization technique. However, in the indoor environments where the NLoS propagation is usually the case, the channel variations with respect to the UE locations are evident, which largely benefits the localization accuracy.

### A. OUTDOOR MEASUREMENT CAMPAIGN

The outdoor measurement campaign consists of two measurements: one for training phase and the other for localization phase. Both measurements were performed in Jiading campus, Tongji University at different days with an interval of one week. Figure 4 illustrates the routes of the two measurements on a satellite-view map and four photographs taken during the measurements. In this map, the yellow and

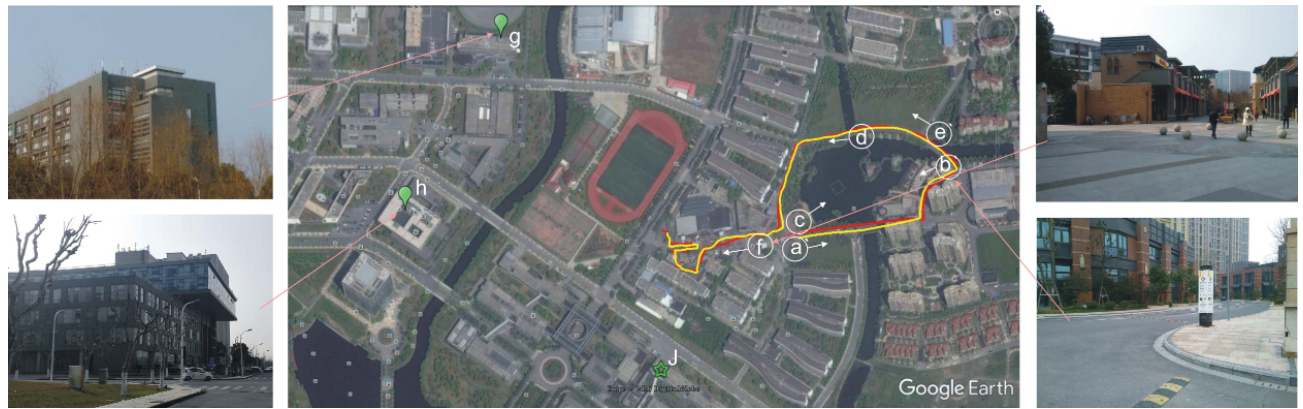


**Fig. 4.** The satellite map of the area of the outdoor measurement campaign.

red lines denote the routes of the first and second measurements respectively. It can be observed that the environment is the typical suburban area in China with largely-separated buildings of height ranging from 7 to 24 storeys.

The sizes of the measurement area as showed in Figure 4 are about 610 meters and 310 meters in the west-east and the north-south directions respectively. Two LTE BSs exist which are located on the rooftop of seven-storey Dianxin Building denoted by “g” and Qiche Building marked with “h” respectively. The marks “a” ~ “f” denote the locations where photographs are taken. The arrow on the circle coincides with the shooting direction of the photograph. The receiver moved at an average pedestrian speed of 1.1 meters per second. The latitude and longitude of the receiver were recorded once per second by using the GPS receiver. It can be observed from the photos taken at the locations “b” and “f” that the measurements were performed along a main road crossing the areas of three-storey shops, seven-storey dormitory buildings, and twenty-storey residential buildings. Light traffic and few people were observed during the measurements. Most of time, a LoS path between the receiver and the BS existed. Situations occurred with the LoS path blocked in the measurements, leading to a batch of NLoS paths. A total of 539 sampling locations of the first measurement are used for training a neural network, while 502 sampling locations of the second measurement are used for test. Note that only one fingerprint vector was generated for each sampling location.

CIRs were extracted from the down-link signals obtained from the same LTE cell during the two measurements. Figure 5 illustrates an example of concatenated normalized PDPs that last for two seconds. Note that the normalization is performed by using (3). It can be observed from Figure 5 that a LoS path is accompanied by some NLoS paths. The power of these NLoS paths changes rapidly during the whole two seconds.

Figure 6 illustrates the empirical contribution to the entropy for all the eleven channel parameters in the first measurement. It is evident from Figure 6 that three channel parameters, namely the standard deviation of RSRP  $\xi_{\sigma_{rsrp}}$ ,

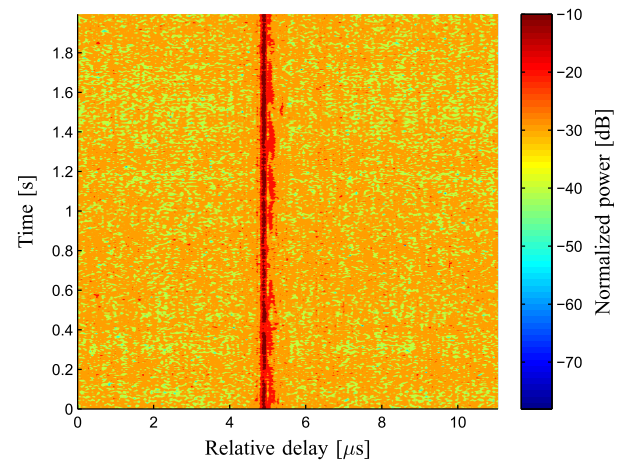


**Fig. 5.** An example of concatenated normalized power delay profiles extracted during the first outdoor measurement.

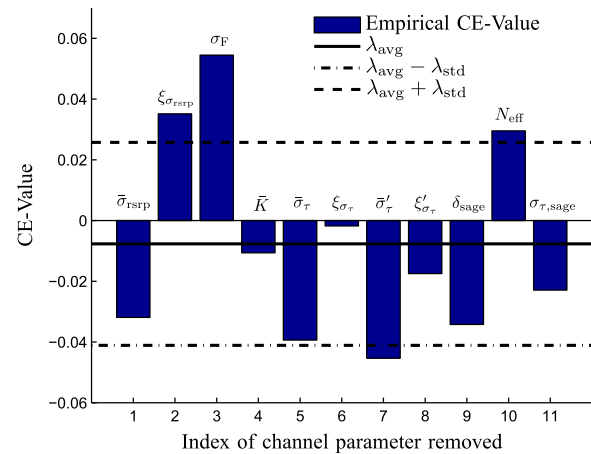


**Fig. 6.** Contribution to the entropy of all the eleven channel parameters in the first outdoor measurement.

the standard deviation of multipath fading  $\sigma_F$  and the average number of effective multipaths  $N_{\text{eff}}$ , can be considered as the entropy-contributing features. This makes sense as these three parameters are closely associated with the surroundings of the

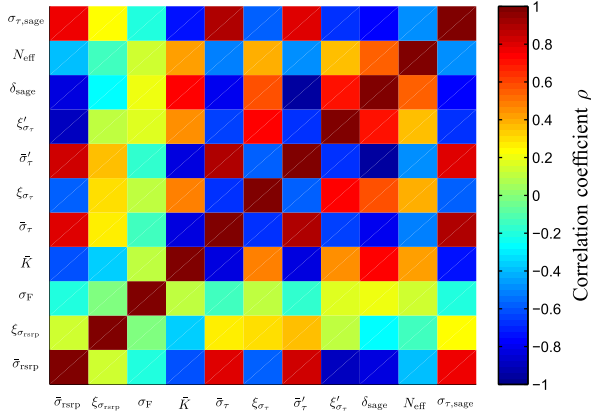


**Fig. 7.** Correlation coefficients among all the eleven channel parameters in the first outdoor measurement.

receiver, and thus, may jointly serve as a unique label of the receiver location. It is also noted that the delay-spread-based parameters do not contribute as much as the other parameters. This is non-surprising since in the outdoor scenarios with the LoS path present, the delay spread does not change significantly as the UE moves, and consequently, they fail to provide the clear and unique identification of the specific environment where the UE resides.

For the first outdoor measurement, the Sammon's errors of the four feature-extraction approaches are calculated. The results show that the four approaches exhibit a common Sammon's error equal to 0.27. It is implied that the three selected channel parameters are non-redundant regardless of the feature-extraction approaches being applied. Figure 7 depicts the correlation coefficients among all the eleven channel parameters calculated by using (21). It can be observed from Figure 7 that the correlation coefficients between  $\xi_{\sigma_{rsrp}}$  and  $\sigma_F$ ,  $\xi_{\sigma_{rsrp}}$  and  $N_{eff}$ ,  $\sigma_F$  and  $N_{eff}$  are 0.007, 0.138, and 0.129 respectively, revealing that they are weakly connected with each other. The values of  $\Lambda$  for the four feature-extraction approaches are obviously the same. Therefore, the three channel parameters, i.e.  $\xi_{\sigma_{rsrp}}$ ,  $\sigma_F$  and  $N_{eff}$ , have been selected as a channel parameter subset for the environment being measured. Based on this result, a fingerprint matrix  $\mathbf{F}'_{tp} \in \mathcal{R}^{539 \times 3}$  and a location matrix  $\mathbf{G}_{tp} \in \mathcal{R}^{539 \times 2}$  are formulated and used to train the neural network. In addition, another fingerprint matrix  $\mathbf{F}'_{lp} \in \mathcal{R}^{502 \times 3}$  and location matrix  $\mathbf{G}_{lp} \in \mathcal{R}^{502 \times 2}$  are formed and applied to evaluating the performance of the localization technique.

To evaluate the accuracy of localization technique, the so-called “positioning error distance” denoted by  $\eta_e$  is applied which is defined as a distance calculated using the true UE location and the estimated location [10]. Specifically, the positioning error distance for each sampling location is calculated based on the difference between the true coordinate of the receiver and its estimate obtained by using the trained neural network. Figure 8 depicts the cumulative distribution function of  $\eta_e$  calculated by using 502 sampling locations, i.e. 502 valid fingerprint vectors in this

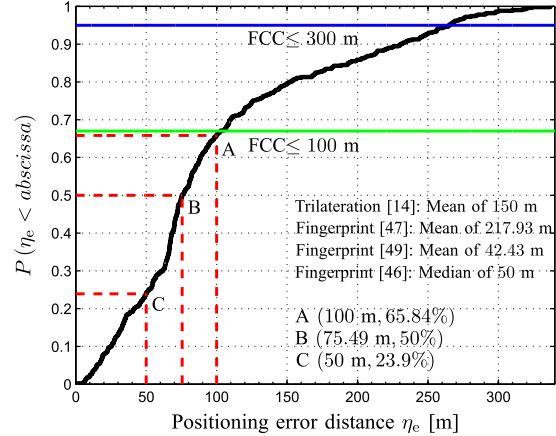


**Fig. 8.** The cumulative distribution function of the positioning error distance obtained in the outdoor measurement campaign.

case. It can be observed that the median of positioning error distance is about 75 meters, and the percentages of locations with  $\eta_e$  less than 50 meters, within the range of [50, 100] meters, and beyond 100 meters are respectively 23.9%, 41.94% and 34.16%. The distribution exhibits a heavy tail to the larger end of the abscissa with the maximal error distance up to 336.8 meters. The Federal Communication Commission (FCC) requires that 67% and 95% of the locations should have positioning error distances of up to 100 meters and 300 meters respectively [76]. As indicated by the green and the blue lines showed in Figure 8, the empirical 67% and 95% of the locations in our case have error distances of 102.9 meters and 264.6 meters respectively. It is obvious that the proposed technique needs to be refined in order to comply with the FCC standards.

## B. INDOOR MEASUREMENT CAMPAIGN

The indoor measurement campaign was performed in a ground-floor hall of the Hua Building in Jiading campus, Tongji University in one day. The building is marked by “J” in Figure 4. The photographs taken during the measurement campaign are illustrated in Figure 9 which show the external and internal surroundings of the building. It can be observed that there exist one reception desk, two vending machines and three plaster-surfaced pillars in this wide hall of the building. It can also be observed in Figure 4 that the Hua Building is closer to the BS on the top of Dianxin Building than that on the top of Qiche Building. Note that the indoor localization for a multi-floor scenario has not been considered in this paper. However, to represent a UE location with additional altitude information, the two-dimensional location coordinate system can be extended into a three-dimensional coordinate system. Besides the first two dimensions denoting the x- and y-axis distances, the third dimension can represent the altitude of the UE by setting a reference horizontal plane.

A total of 58 sampling locations were fixedly measured in the area of about 400 square meters, and 410 fingerprint vectors were obtained from all the sampling locations. We randomly chose 80 vectors for the training phase while

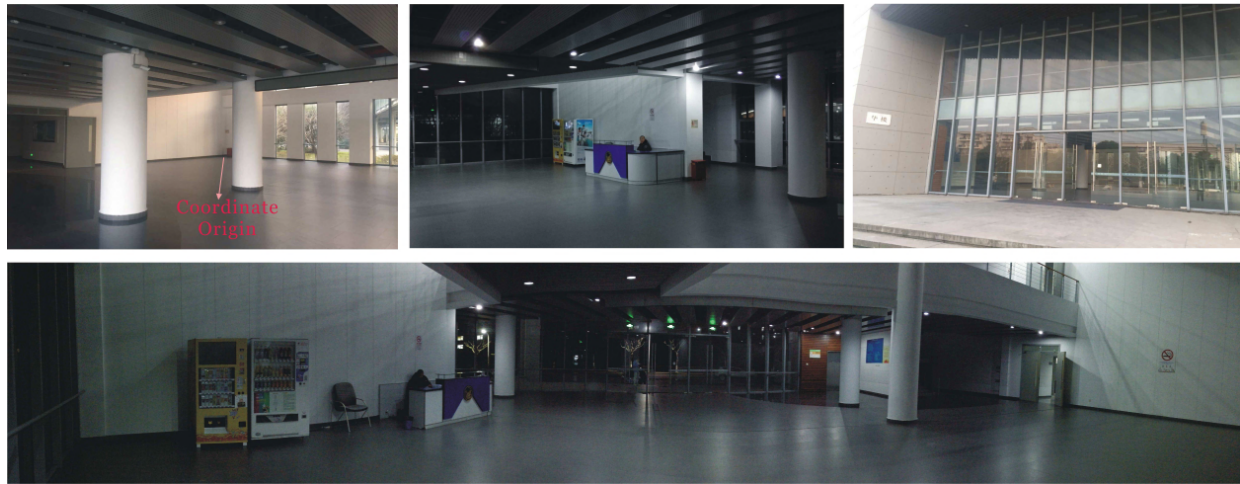


**Fig. 9.** The photographs taken in the indoor measurement area.

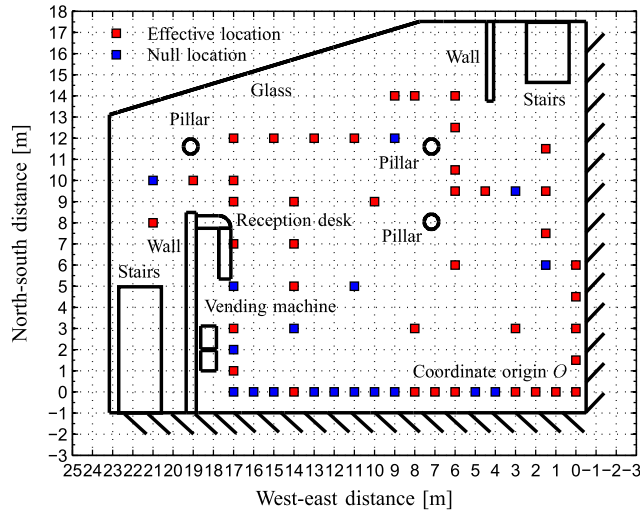


**Fig. 10.** The bird's-eye view map of the indoor measurement area.

the rest of 330 vectors for the localization phase. Figure 10 shows a bird's-eye view map of the ground-floor hall where each of sampling locations is marked by a diamond and main objects in the hall are depicted. In this map, the “Effective location” means that CIRs can be obtained in the current sampling location, while the “Null location” denotes that no valid CIRs have been obtained. It can be observed from Figure 10 that the distance between two adjacent sampling locations is set 1, 1.5 or 2 meters, respectively.

Similar steps to those applied in the outdoor scenario were performed including the parameter selection, the neural network training and the UE localization. Figure 11 illustrates an example of one snapshot of normalized PDP obtained in the indoor measurement campaign. Note that the power threshold in the PDP is set 10 dB below the maximal power to extract the significant channel components.

Figure 12 illustrates the empirical contribution to the entropy for all the eleven channel parameters obtained for

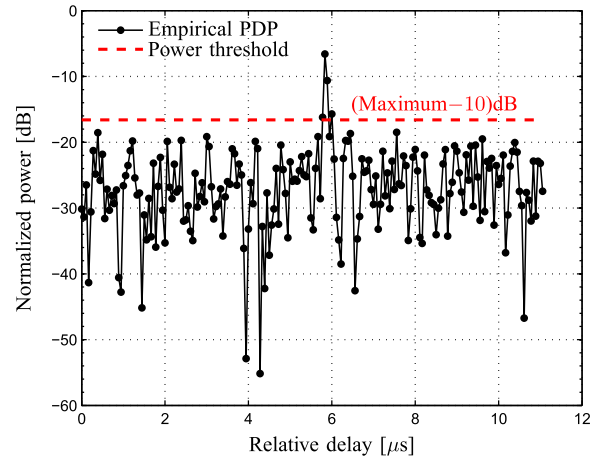


**Fig. 11.** An example of one snapshot of normalized power delay profile extracted from the data of the indoor measurement campaign.

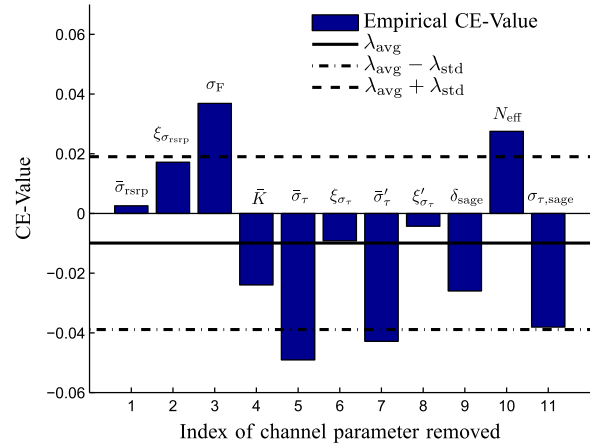


**Fig. 12.** Contribution to the entropy of all the eleven channel parameters obtained in the training phase of indoor measurement campaign.

the sampling locations in the training period of the indoor measurement campaign. It is obvious from Figure 12 that two channel parameters, namely the standard deviation of

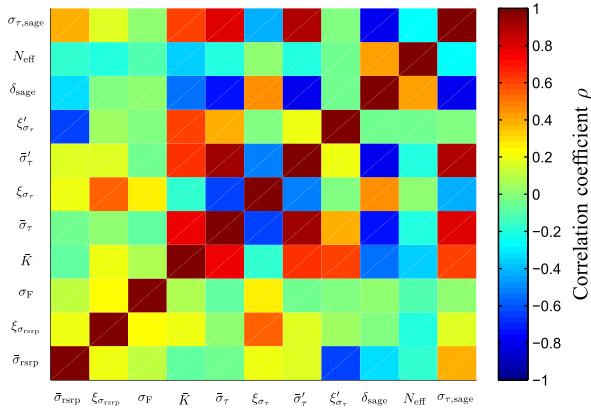


**Fig. 13.** Correlation coefficients among all the eleven channel parameters obtained in the training phase of indoor measurement campaign.

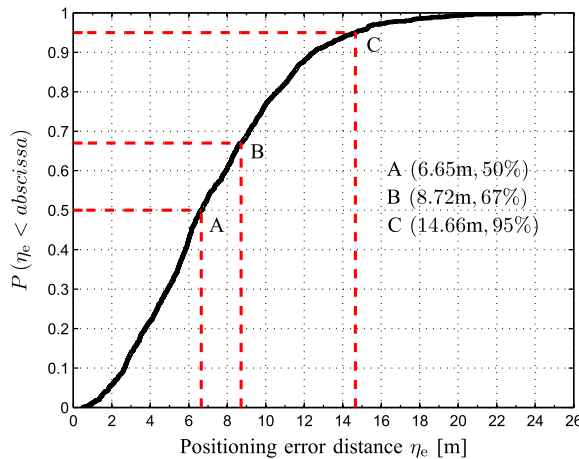


**Fig. 14.** The cumulative distribution function of the positioning error distance obtained in the indoor measurement campaign.

multipath fading  $\sigma_F$  and the average number of effective multipaths  $N_{eff}$ , can be considered as the entropy-contributing features. The results of the SR and the FS2 approaches show that the parameters  $\sigma_F$  and  $N_{eff}$  can be selected as a channel parameter subset. However, the result of the FS1 approach shows that the parameters  $\sigma_F$  and  $\delta_{sage}$  are supposed to be chosen while the BE approach tends to select the parameters  $\bar{\sigma}_{rsrp}$  and  $\sigma_F$ .

Figure 13 depicts the correlation coefficients among all the eleven parameters during the training phase in the indoor measurement campaign. It can be observed from Figure 13 that the correlation coefficients between  $\sigma_F$  and  $N_{eff}$ ,  $\sigma_F$  and  $\delta_{sage}$ , as well as  $\bar{\sigma}_{rsrp}$  and  $\sigma_F$  are  $-0.12$ ,  $0.012$  and  $0.106$  respectively. The values of  $\Lambda$  for four feature-extraction approaches are  $0.5224$ ,  $0.3998$ ,  $0.5224$  and  $0.4943$  respectively. As a consequence, the two channel parameters given by the FS1 approach, i.e.  $\sigma_F$  and  $\delta_{sage}$  have been selected as a channel parameter subset for the environment being measured.

Figure 14 depicts the cumulative distribution function of positioning error distance  $\eta_e$  obtained through 324 valid fingerprint vectors in 40 effective sampling locations of the indoor measurement campaign.

**TABLE 4.** Summarized results of localization technique validation obtained from the two measurement campaigns.

Term \ Scenario	Indoor	Outdoor
Scene Feature	A wide ground-floor building hall	A campus in suburban area
Measurement Area Coverage	About 400 square meters	About 0.18 square kilometers
Sammon's Error	0.4026 for SR/FS2 0.3875 for FS1 0.3887 for BE	0.27 for SR/FS1/FS2/BE
Correlation Coefficient	$\sigma_F \& N_{eff} : -0.12$ $\sigma_F \& \delta_{sage} : 0.012$ $\bar{\sigma}_{rsrp} \& \sigma_F : 0.106$	$\xi_{\sigma_{rsrp}} \& \sigma_F : 0.007$ $\xi_{\sigma_{rsrp}} \& N_{eff} : 0.138$ $\sigma_F \& N_{eff} : 0.129$
Metric $\Lambda$	0.5224 for SR/FS2 0.3998 for FS1 0.4943 for BE	0.5451 for SR/FS1/FS2/BE
Finally Selected Parameters	$\sigma_F, \delta_{sage}$	$\xi_{\sigma_{rsrp}}, \sigma_F, N_{eff}$
Median Positioning Error Distance	About 6 meters	About 75 meters

SR: Simple Ranking, FS1: the first Forward Selection, FS2: the second Forward Selection, BE: Backward Elimination.

Eventually, to illustrate the performance validation of the proposed localization technique more clearly, Table 4 reports the experimental results obtained in the outdoor and indoor measurement campaigns.

### C. COMPARISONS OF THE PROPOSED TECHNIQUE WITH THE EXISTING METHODS

Compared to the existing localization techniques as reported in Table 1, our proposed CIR-based technique owns the following properties: *i*) it focuses on the channel characteristics that provide a deep understanding of propagation environments; *ii*) it chooses the suitable channel parameters to construct the fingerprint through a feature-extraction algorithm; *iii*) it requires no calibration for the UE side. In indoor environments, the UE may behave more “omni-directionally” due to multiple reflections, and hence needs no calibration of different antennas. In outdoor environments, the UE is more likely to behave “directionally”. However, if a large amount of user equipment data with various states of antennas is collected, the UE localization can be performed in a statistical way, and thus requires no calibration.

It can be observed from Table 1 that in the outdoor scenarios, the minimal positioning error distances are  $42.43$  and  $27.86$  meters for rural and urban cases respectively [49], which are less than the error distance obtained by using our proposed technique. However, the localization technique in [49] needs to execute the two time-consuming matching algorithms, i.e. a probabilistic algorithm for the UE to obtain a sufficient number of samples, and a so-called

*k*NN algorithm requiring the inputs of up to seven physical cells. For the indoor scenarios, the minimal positioning error distance of down to 1 meter can be achieved by using the existing techniques [41], [43], [45], [48]. However, these techniques usually own a high computational complexity. For example, the neural network algorithm proposed in [41] has 45 input neurons, 65 hidden neurons, and 1 output neuron. Moreover, the numbers of input-layer-neurons and hidden-layer-neurons are respectively 4 and 6 times of the numbers in our proposed localization technique. We consider the performance of our technique to be acceptable for a trade-off among the localization accuracy, the technique's complexity as well as the overall time and resource consumption.

## VI. CONCLUSIONS

In this paper, a novel signal fingerprint composed of radio channel characteristics was introduced which provided unique identities for geographical locations of user equipments (UEs) in Long-Term-Evolution (LTE) networks. This fingerprint is a vector consisting of channel parameters that are selected from eleven candidates through a feature-extraction algorithm by assessing their irrelevance and non-redundancy. A feed-forward three-layer neural network using the Levenberg-Marquardt learning algorithm was trained to match a fingerprint matrix to a location matrix. The UE localization can be readily performed by applying the trained neural network. Preliminary experimental results obtained through channel measurements in in-service LTE networks demonstrated that the proposed localization technique yielded median positioning error distances of 6 meters for indoor and of 75 meters for outdoor scenarios respectively. Although such performances do not prevail upon many existing works, the applicability of implementing learning-based strategies in e.g. UE positioning has been demonstrated in this paper with resources available in public wireless communication networks.

## ACKNOWLEDGMENT

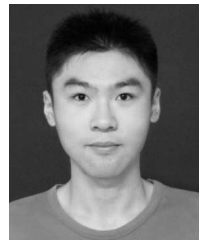
The authors would like to express their thankfulness to Mr. Jiajing Chen and Mr. Yilin Ji from Tongji University for their valuable comments on this paper.

## REFERENCES

- [1] N. M. Drawil and O. Basir, "Intervehicle-communication-assisted localization," *IEEE Trans. Intell. Trans. Syst.*, vol. 11, no. 3, pp. 678–691, Sep. 2010.
- [2] D. M. Ashok, M. M. M. Pai, and J. Mouzna, "Efficient map based location service for VANETs," in *Proc. 11th Int. Conf. ITS Telecommun.*, Aug. 2011, pp. 387–392.
- [3] R. Filjar, M. Sevrovic, and I. Dadic, "Positioning and localisation for location-based services," in *Proc. 21st Telecommun. Forum*, Nov. 2013, pp. 9–12.
- [4] M. Zhou, A. K. S. Wong, Z. Tian, X. Luo, K. Xu, and R. Shi, "Personal mobility map construction for crowd-sourced Wi-Fi based indoor mapping," *IEEE Commun. Lett.*, vol. 18, no. 8, pp. 1427–1430, Aug. 2014.
- [5] X. Lu, H. Zou, H. Zhou, L. Xie, and G.-B. Huang, "Robust extreme learning machine with its application to indoor positioning," *IEEE Trans. Cybern.*, vol. 46, no. 1, pp. 194–205, Jan. 2016.
- [6] Y. Cui and S. S. Ge, "Autonomous vehicle positioning with GPS in urban canyon environments," *IEEE Trans. Robot. Autom.*, vol. 19, no. 1, pp. 15–25, Feb. 2003.
- [7] U. Blanke, G. Troster, T. Franke, and P. Lukowicz, "Capturing crowd dynamics at large scale events using participatory GPS-localization," in *Proc. 9th Int. Conf. Intell. Sensors, Sensor Netw. Inf. Process.*, Apr. 2014, pp. 1–7.
- [8] H. Qin, L. Cong, and X. Sun, "Accuracy improvement of GPS/MEMS-INS integrated navigation system during GPS signal outage for land vehicle navigation," *J. Syst. Eng. Electron.*, vol. 23, no. 2, pp. 256–264, Apr. 2012.
- [9] F. Gustafsson and F. Gunnarsson, "Mobile positioning using wireless networks: Possibilities and fundamental limitations based on available wireless network measurements," *IEEE Signal Process. Mag.*, vol. 22, no. 4, pp. 41–53, Jul. 2005.
- [10] H. Liu, H. Darabi, P. Banerjee, and J. Liu, "Survey of wireless indoor positioning techniques and systems," *IEEE Trans. Syst., Man, Cybern. C, Appl. Rev.*, vol. 37, no. 6, pp. 1067–1080, Nov. 2007.
- [11] S. Mazuelas *et al.*, "Robust indoor positioning provided by real-time RSSI values in unmodified WLAN networks," *IEEE J. Sel. Topics Signal Process.*, vol. 3, no. 5, pp. 821–831, Oct. 2009.
- [12] S. Shrestha, E. Laitinen, J. Talvitie, and E. S. Lohan, "RSSI channel effects in cellular and WLAN positioning," in *Proc. 9th Workshop Positioning Navigat. Commun. (WPNC)*, Mar. 2012, pp. 187–192.
- [13] A. Prasad, P. Lunden, O. Tirkkonen, and C. Wijting, "Energy efficient small-cell discovery using received signal strength based radio maps," in *Proc. IEEE 77th Veh. Technol. Conf. (VTC Spring)*, Jun. 2013, pp. 1–5.
- [14] M. Pent, M. A. Spirito, and E. Turco, "Method for positioning GSM mobile stations using absolute time delay measurements," *Electron. Lett.*, vol. 33, no. 24, pp. 2019–2020, Nov. 1997.
- [15] C. Mensing and S. Plass, "Positioning algorithms for cellular networks using TDOA," in *Proc. IEEE Int. Conf. Acoust., Speech Signal Process.*, vol. 4, May 2006, p. 4.
- [16] F. Izquierdo, M. Ciurana, F. Barcelo, J. Paradells, and E. Zola, "Performance evaluation of a TOA-based trilateration method to locate terminals in WLAN," in *Proc. 1st Int. Symp. Wireless Pervasive Comput.*, Jan. 2006, pp. 1–6.
- [17] D. E. Manolakis, "Efficient solution and performance analysis of 3-D position estimation by trilateration," *IEEE Trans. Aerosp. Electron. Syst.*, vol. 32, no. 4, pp. 1239–1248, Oct. 1996.
- [18] B. D. Van Veen and K. M. Buckley, "Beamforming: A versatile approach to spatial filtering," *IEEE ASSP Mag.*, vol. 5, no. 2, pp. 4–24, Apr. 1988.
- [19] H. Tsuji, "Radio location estimation using signal subspaces of array antennas," in *Proc. Int. Symp. Intell. Signal Process. Commun. Syst. (ISPACS)*, Jan. 2009, pp. 244–247.
- [20] V. Honkavirta, T. Perala, S. Ali-Loytty, and R. Piche, "A comparative survey of WLAN location fingerprinting methods," in *Proc. 6th Workshop Positioning, Navigat. Commun.*, Mar. 2009, pp. 243–251.
- [21] Q. D. Vo and P. De, "A survey of fingerprint-based outdoor localization," *IEEE Commun. Surveys Tuts.*, vol. 18, no. 1, pp. 491–506, First Quart., 2016.
- [22] M. Azizyan, I. Constandache, and R. R. Choudhury, "Surround-Sense: Mobile phone localization via ambience fingerprinting," in *Proc. 15th Annu. Int. Conf. Mobile Comput. Netw.*, New York, NY, USA, 2009, pp. 261–272. [Online]. Available: <http://doi.acm.org/10.1145/1614320.1614350>
- [23] G. Schroth, R. Huitl, D. Chen, M. Abu-Alqumsan, A. Al-Nuaimi, and E. Steinbach, "Mobile visual location recognition," *IEEE Signal Process. Mag.*, vol. 28, no. 4, pp. 77–89, Jul. 2011.
- [24] T.-N. Lin and P.-C. Lin, "Performance comparison of indoor positioning techniques based on location fingerprinting in wireless networks," in *Proc. Int. Conf. Wireless Netw. Commun. Mobile Comput.*, vol. 2, Jun. 2005, pp. 1569–1574.
- [25] M. Ibrahim and M. Youssef, "Cellsense: A probabilistic RSSI-based GSM positioning system," in *Proc. IEEE Global Telecommun. Conf.*, Dec. 2010, pp. 1–5.
- [26] C. Feng, W. S. A. Au, S. Valaee, and Z. Tan, "Received-signal-strength-based indoor positioning using compressive sensing," *IEEE Trans. Mobile Comput.*, vol. 11, no. 2, pp. 1983–1993, Dec. 2012.
- [27] H. Buyruk *et al.*, "RF fingerprinting based GSM indoor localization," in *Proc. 21st Signal Process. Commun. Appl. Conf.*, Apr. 2013, pp. 1–4.
- [28] R. M. Vaghefi and R. Buehrer, "Cooperative RF pattern matching positioning for LTE cellular systems," in *Proc. 25th Annu. Int. Symp. Pers., Indoor, Mobile Radio Commun. (PIMRC)*, Sep. 2014, pp. 264–269.

- [29] V. Savic and E. G. Larsson, "Fingerprinting-based positioning in distributed massive MIMO systems," in *Proc. IEEE 82nd Veh. Technol. Conf. (VTC Fall)*, Sep. 2015, pp. 1–5.
- [30] C. Nerguizian and V. Nerguizian, "Indoor fingerprinting geolocation using wavelet-based features extracted from the channel impulse response in conjunction with an artificial neural network," in *Proc. IEEE Int. Symp. Ind. Electron.*, Jun. 2007, pp. 2028–2032.
- [31] N. A. Khanbashi et al., "Real time evaluation of RF fingerprints in wireless LAN localization systems," in *Proc. 10th Workshop Positioning Navigat. Commun.*, Mar. 2013, pp. 1–6.
- [32] N. Alsindi, Z. Chaloupka, N. AlKhanbashi, and J. Aweya, "An empirical evaluation of a probabilistic RF signature for WLAN location fingerprinting," *IEEE Trans. Wireless Commun.*, vol. 13, no. 6, pp. 3257–3268, Jun. 2014.
- [33] J. Paek, K.-H. Kim, J. P. Singh, and R. Govindan, "Energy-efficient positioning for smartphones using cell-ID sequence matching," in *Proc. 9th Int. Conf. Mobile Syst., Appl., Services*, New York, NY, USA, 2011, pp. 293–306. [Online]. Available: <http://doi.acm.org/10.1145/1999995.2000024>
- [34] C. Wu, Z. Yang, Y. Liu, and W. Xi, "WILL: Wireless indoor localization without site survey," *IEEE Trans. Parallel Distrib. Syst.*, vol. 24, no. 4, pp. 839–848, Apr. 2013.
- [35] P. Kontkanen, P. Myllymaki, T. Roos, H. Tirri, K. Valtonen, and H. Wettig, "Topics in probabilistic location estimation in wireless networks," in *Proc. 15th IEEE Int. Symp. Pers., Indoor Mobile Radio Commun. (PIMRC)*, vol. 2, Sep. 2004, pp. 1052–1056.
- [36] M. Brunato and R. Battiti, "Statistical learning theory for location fingerprinting in wireless LANs," *Comput. Netw.*, vol. 47, no. 6, pp. 825–845, 2005.
- [37] O. M. Badawy and M. A. B. Hasan, "Decision tree approach to estimate user location in WLAN based on location fingerprinting," in *Proc. 24th Nat. Radio Sci. Conf.*, Mar. 2007, pp. 1–10.
- [38] M. Roshanaei and M. Maleki, "Dynamic-KNN: A novel locating method in WLAN based on angle of arrival," in *Proc. IEEE Symp. Ind. Electron. Appl. (ISIEA)*, vol. 2, Oct. 2009, pp. 722–726.
- [39] S. Dayekh, S. Affes, N. Kandil, and C. Nerguizian, "Cooperative geolocation in underground mines: A novel fingerprint positioning technique exploiting spatio-temporal diversity," in *Proc. 22nd Int. Symp. Pers. Indoor Mobile Radio Commun. (PIMRC)*, Sep. 2011, pp. 1319–s1324.
- [40] L. Qiu and R. A. Kennedy, "Radio location using pattern matching techniques in fixed wireless communication networks," in *Proc. Int. Symp. Commun. Inf. Technol.*, Oct. 2007, pp. 1054–1059.
- [41] L. Leins and C. Steiner, "Neural network based Geo-regioning," in *Proc. IEEE Int. Conf. Ultra-Wideband (ICUWB)*, vol. 2, Sep. 2008, pp. 229–232.
- [42] Y. Jin, W.-S. Soh, and W.-C. Wong, "Indoor localization with channel impulse response based fingerprint and nonparametric regression," *IEEE Trans. Wireless Commun.*, vol. 9, no. 3, pp. 1120–1127, Mar. 2010.
- [43] S. Dayekh, S. Affes, N. Kandil, and C. Nerguizian, "Cooperative localization in mines using fingerprinting and neural networks," in *Proc. IEEE Wireless Commun. Netw. Conf. (WCNC)*, Apr. 2010, pp. 1–6.
- [44] N. Khanbashi, N. Alsindi, S. Al-Araji, N. Ali, and J. Aweya, "Performance evaluation of CIR based location fingerprinting," in *Proc. 23rd Int. Symp. Pers. Indoor Mobile Radio Commun. (PIMRC)*, Sep. 2012, pp. 2466–2471.
- [45] Y. P. Lin, P. H. Tseng, and K. T. Feng, "Compressive sensing based location estimation using channel impulse response measurements," in *Proc. 25th Annu. Int. Symp. Pers., Indoor, Mobile Radio Commun. (PIMRC)*, Sep. 2014, pp. 2066–2070.
- [46] A. Haniz et al., "Localization of illegal radios utilizing cross-correlation of channel impulse response with interpolation in urban scenarios," in *Proc. IEEE Military Commun. Conf.*, Oct. 2015, pp. 210–215.
- [47] S. Ergut, R. R. Rao, and O. Dural, "Localization via multipath strengths in a CDMA2000 cellular network using neural networks," in *Proc. IEEE Int. Joint Conf. Neural Netw. (IJCNN), (IEEE World Congr. Computat. Intell.)*, Jun. 2008, pp. 4066–4069.
- [48] A. Szabo, T. Weiherer, and J. Bamberger, "Unsupervised learning of propagation time for indoor localization," in *Proc. 73rd Veh. Technol. Conf. (VTC Spring)*, May 2011, pp. 1–5.
- [49] M. Ibrahim and M. Youssef, "Cellsense: An accurate energy-efficient GSM positioning system," *IEEE Trans. Veh. Technol.*, vol. 61, no. 1, pp. 286–296, Jan. 2012.
- [50] T. Wigren, "Clustering and polygon merging algorithms for fingerprinting positioning in LTE," in *Proc. 5th Int. Conf. Signal Process. Commun. Syst.*, Dec. 2011, pp. 1–10.
- [51] R. Mondal, J. Turkka, T. Ristaniemi, and T. Henttonen, "Performance evaluation of MDT assisted LTE RF fingerprint framework," in *Proc. 7th Int. Conf. Mobile Comput. Ubiquitous Netw.*, Jan. 2014, pp. 33–37.
- [52] X. Ye, X. Cai, Y. Shen, X. Yin, and X. Cheng, "A geometry-based path loss model for high-speed-train environments in LTE-A networks," in *Proc. Int. Conf. Comput., Netw. Commun. (ICNC)*, Feb. 2016, pp. 1–6.
- [53] B. H. Fleury, M. Tschudin, R. Heddergott, D. Dahlhaus, and K. Ingeman Pedersen, "Channel parameter estimation in mobile radio environments using the SAGE algorithm," *IEEE J. Sel. Areas Commun.*, vol. 17, no. 3, pp. 434–450, Mar. 1999.
- [54] X. Yin and X. Cheng, *Propagation Channel Characterization, Parameter Estimation and Modelling for Wireless Communications*. Hoboken, NJ, USA: Wiley, 2016.
- [55] *LTE; Evolved Universal Terrestrial Radio Access (E-UTRA); Physical Channels and Modulation*, 3rd Generation Partnership Project (3GPP), Version 12.5.0 Release 12 document TS 36.211, ETSI, Apr. 2015.
- [56] A. Goldsmith, *Wireless Communicaitons*. Cambridge, U.K.: Cambridge Univ. Press, 2005.
- [57] A. F. Molisch, *Wireless Communications*. Hoboken, NJ, USA: Wiley, 2011.
- [58] H. Hashemi and D. Tholl, "Statistical modeling and simulation of the RMS delay spread of indoor radio propagation channels," *IEEE Trans. Veh. Technol.*, vol. 43, no. 1, pp. 110–120, Feb. 1994.
- [59] H. Hashemi, "The indoor radio propagation channel," *Proc. IEEE*, vol. 81, no. 7, pp. 943–968, Jul. 1993.
- [60] J. C. Ang, A. Mirza, H. Haron, and H. N. A. Hamed, "Supervised, unsupervised, and semi-supervised feature selection: A review on gene selection," *IEEE/ACM Trans. Comput. Biol. Bioinf.*, vol. 13, no. 5, pp. 971–989, Sep. 2016.
- [61] L. Yu and H. Liu, "Efficient feature selection via analysis of relevance and redundancy," *J. Mach. Learn. Res.*, vol. 5, no. 10, pp. 1205–1224, 2004.
- [62] Q. Zuo, X. Yin, Z. Zeng, B. J. Kwak, and H. K. Chung, "Experimental spatial correlation characteristics of propagation channels in indoor environments," in *Proc. Int. Conf. Wireless Commun. Signal Process.*, Oct. 2010, pp. 1–5.
- [63] O. Alter, P. O. Brown, and D. Botstein, "Singular value decomposition for genome-wide expression data processing and modeling," *Proc. Nat. Acad. Sci. USA*, vol. 97, no. 18, pp. 10101–10106, Aug. 2000.
- [64] R. Varshavsky, A. Gottlieb, and D. Horn, "Novel unsupervised feature filtering of biological data," *Bioinformatics*, vol. 22, no. 14, pp. e507–e513, 2006.
- [65] M. Banerjee and N. R. Pal, "Feature selection with SVD entropy: Some modification and extension," *Inf. Sci.*, vol. 264, pp. 118–134, Apr. 2014. [Online]. Available: <http://www.sciencedirect.com/science/article/pii/S0020025513008797>
- [66] X. Yin et al., "Modeling city-canyon pedestrian radio channels based on passive sounding in in-service networks," *IEEE Trans. Veh. Technol.*, vol. 65, no. 10, pp. 7931–7943, Oct. 2016.
- [67] R. P. Lippmann, "An introduction to computing with neural nets," *IEEE ASSP Mag.*, vol. 4, no. 2, pp. 4–22, Apr. 1987.
- [68] R. Zouari, I. Ahriz, R. Zayani, A. Dziri, and R. Bouallegue, "Relevant CIR parameters selection for fingerprinting based location algorithm," in *23rd Int. Conf. Softw., Telecommun. Comput. Netw.*, Sep. 2015, pp. 170–173.
- [69] M. Kalakh, N. Kandil, and N. Hakem, "Neural networks model of an UWB channel path loss in a mine environment," in *Proc. IEEE 75th Veh. Technol. Conf. (VTC Spring)*, May 2012, pp. 1–5.
- [70] T. Guo and G.-Y. Li, "Neural data mining for credit card fraud detection," in *Proc. Int. Conf. Mach. Learn.*, vol. 7, Jul. 2008, pp. 3630–3634.
- [71] D. E. Rumelhart, G. E. Hinton, and R. J. Williams, "Learning representations by back-propagating errors," *Nature*, vol. 323, pp. 533–536, Oct. 1986.
- [72] B. M. Wilamowski, "Neural network architectures and learning algorithms," *IEEE Ind. Electron. Mag.*, vol. 3, no. 4, pp. 56–63, Dec. 2009.
- [73] H. Yu and B. M. Wilamowski, "Efficient and reliable training of neural networks," in *Proc. 2nd Conf. Human Syst. Interact.*, May 2009, pp. 109–115.
- [74] M. T. Hagan and M. B. Menhaj, "Training feedforward networks with the Marquardt algorithm," *IEEE Trans. Neural Netw.*, vol. 5, no. 6, pp. 989–993, Nov. 1994.

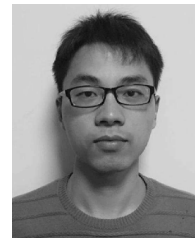
- [75] B. M. Wilamowski, N. J. Cotton, O. Kaynak, and G. Dundar, "Computing gradient vector and Jacobian matrix in arbitrarily connected neural networks," *IEEE Trans. Ind. Electron.*, vol. 55, no. 10, pp. 3784–3790, Oct. 2008.
- [76] C. L. F. Mayorga *et al.*, "Cooperative positioning techniques for mobile localization in 4G cellular networks," in *Proc. IEEE Int. Conf. Pervas. Services*, Jul. 2007, pp. 39–44.



**XIAOKANG YE** (S'16) received the bachelor's degree in electrical engineering from the Shanghai University of Engineering Science, Shanghai, China, in 2014. He is currently pursuing the Ph.D. degree with the College of Electronics and Information Engineering, Tongji University. His research interests include statistical channel characterization, millimeter wave channel characterization and modeling, channel fingerprint, and applications of machine learning-based techniques on propagation channel characterization.



**XUEFENG YIN** (S'01–M'06) received the bachelor's degree in optoelectronics engineering from the Huazhong University of Science and Technology, Wuhan, China, in 1995, and the M.Sc. degree in digital communications and the Ph.D. degree in wireless communications from Aalborg University, Denmark, in 2002 and 2006, respectively. From 2006 to 2008, he was an Assistant Professor with Aalborg University. In 2008, he joined the College of Electronics and Information Engineering, Tongji University, Shanghai, China. He became a Full Professor in 2016 and served as the Vice Dean for the College of Electronics and Information Engineering. He has published about 100 technical papers and co-authored the book "*Propagation Channel Characterization, Parameter Estimation and Modeling for Wireless Communications*" (John Wiley and Sons Edition, 2016). His research interests include high-resolution parameter estimation for propagation channels, measurement-based channel characterization and stochastic modeling for 5G wireless communications, channel simulation based on random graph models, radar signal processing, and target recognition.



**XUESONG CAI** (S'14) received the bachelor's degree in electronics science and technology from Tongji University, Shanghai, China, in 2013, where he is currently pursuing the Ph.D. degree with the College of Electronics and Information Engineering. His research interests include passive channel sounding and time-variant channel characterization and modeling.



**ANTONIO PÉREZ YUSTE** (M'03–SM'11) was born in Toledo, Spain, in 1968. He received the B.Eng. degree in radiocommunications, the M.Eng. degree in telecommunications, and the Ph.D. (cum laude) degree in telecommunications from the Technical University of Madrid (UPM), Spain, in 1991, 1996, and 2004, respectively. He has held different academic positions with the Technical University of Madrid. He was a Vice Director of the School of Telecommunications with UPM from 1997 to 2001, where he was also the Director from 2001 to 2004, and the Head of the UPM President's Cabinet from 2004 to 2012. He was the UPM Sino-Spanish Campus Director in Shanghai, China, from 2012 to 2014. In 2014, he was in charge of the UPM Sino-Spanish Cooperation Office in Madrid. He is currently a Professor of telecommunications engineering with the Technical University of Madrid. In addition, he is a Specialist in the history of electrical and electronic engineering, with special emphasis on the history of telecommunications and the development of the Information Society. His current research interests are related to radio propagation and channel modeling.



**HONGLIANG XU** received the bachelor's degree in communication engineering from Shanghai University, Shanghai, China, in 2003, and the M.Eng. degree in electronics and communication engineering from Fudan University, Shanghai, China, in 2010. He is currently with Shanghai Radio Monitoring Station and responsible for the radio monitoring and direction finding. His research interests are radio determination and location with multipath channels.